Aerodynamic optimisation of a front wheel wake related bodywork on a novel electric formula car using metaheuristic approach

Authors: Miklos Diosy and Daniel Bell

Abstract

Aerodynamic drag reduction is a critical part in the design of a novel electric, entry level, formula car due to the modest energy density provided by the contemporary Lithium-ion battery cells. In order to improve track performance, aerodynamic development must focus on components which do not generate considerable amount of downforce. Rotating front wheels are identified as the least aerodynamic part of the race car, since it is responsible for the third of the overall drag forces and producing moderate amounts of lift. In the present study, a parameterised wheel pod geometry is used to improve the overall aerodynamic performance of an open wheel race car. The model is driven by seven parameters, which entails huge flexibility of the bodywork design. First, an unsteady Computational Fluid Dynamics (CFD) simulation was developed and validated to visualise the oscillating flow behaviour and obtain averaged surface force measurements. In expectation of a highly turbulent and complex wheel wake structure, the traditional iterative optimisation method had to be excluded. The exploration of the optimal bodywork was executed by a single objective aerodynamic optimisation framework, coupled with CFD simulations. The objective target was to minimise overall drag force while the simulation must agree on the pre-set restrictions and leave downforce unharmed. SHERPA search algorithm was applied along with Kriging response surface surrogate modelling. The convergence of the objective history indicated acceptable fidelity of the predictions for the location of the global minimum of the 8-dimension design space. The race car equipped with the best design wheel pod generated 11.1% less overall drag, while aerodynamic efficiency was improved by 17.1%.

Introduction

Application of all-electric powertrains are becoming more and more popular among passenger and motorsport vehicles. According to a 2017 study of Maroti [1], 78% of UK based mid-level motorsport team owners were rather positive about electric competition cars. Thereof 30% believed electric vehicles are indeed the future of motorsport.

Formula Club E (FCE) in collaboration with Oxford Brookes University is an entry level electric formula car project, which is intended to fulfil the market need between electric karting and Formula E championship (Figure 1). In previous works within the FCE project, underbody and drivetrain were optimised to produce competitive overall performance based on LTSs on selected UK race tracks. The amount of generated downforce and the characteristics of the associated aeromaps are acceptable, along with the longitudinal acceleration. Albeit, current range could be the barrier of FCE's success and popularity among other conventional internal combustion competition series. FCE such as other race cars with all-electric powertrain has to balance between the amount of utilised Lithium-ion battery cells, race track performance (eg. acceleration, range etc.) and selling price. Due to the relatively low energy per unit mass and high price of the present technology battery packs, longitudinal drag levels are identified as significant limiter in terms of vehicle performance and overall competitiveness.

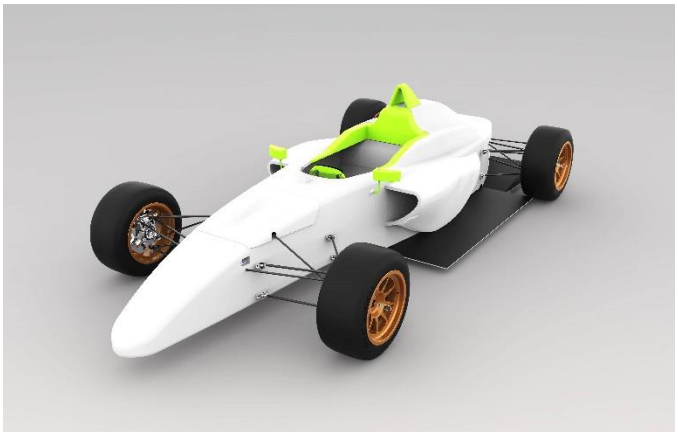

Figure 1. Fully-electric Formula Club E baseline car (Source: [2])

The aerodynamic performance development of the FCE car should be focused upon components of the car, which do not generate reasonable amount of favourable downforce according to the work of Sprot et al. [3]. Exposed rotating front wheels of formula type race cars can contribute between 35% and 50% towards the overall aerodynamic drag [4], while they have between 0.35 and 0.44 positive lift coefficient [5]. Aerodynamic drag and lift are both undesirable forces, due to their detrimental effect on straight line and cornering performance in sequence. Therefore, reducing aerodynamic drag and lift by a locally placed wake flow modifying wheel pod is a logical decision for open wheel race cars; this is typically observed to be the case in present day Formula-E.

The idea to reduce wheel drag by partial coverage of rim or fairing can be found among the experiments of Paul Jaray in the 1920's and from the dawn of aeronautics [6].

Although, wheel related bodyworks were virtually absent during the history of popular open-wheeled race series (eg. Formula 1 and IndyCar), prohibited by race regulations. The intention behind this was to preserve the layout of traditional formula type cars, hence to balance the exponentially growing power output of the internal combustion engine with drag levels.

The introduction of Formula E series has changed this classical judgement drastically. Teams are encountering very similar problems due to low energy density of present battery cells. Figure 2 shows wheel related bodyworks. Primarily, these components are used to minimise the possibility of dangerous wheel-to-wheel contacts during races. Additionally, they contribute to reductions in drag levels of the cars, however there is little published data concerning the effects and gains obtained.

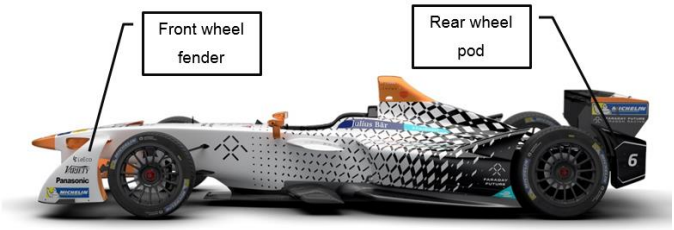

Figure 2. Wheel wake related bodyworks on a modern Formula E competition car

Aerodynamic investigations of isolated rotating wheel

The drag forces acting on an exposed rotating wheel assembly is the sum of normal pressure, skin friction and induced drag. By its very nature, induced drag has its major importance, due to an adverse, low pressure flow region, formed behind the wheel, called wheel wake zone. This fairly complex flow system is generating more drag through interaction with other body parts of the car. Despite the evident and pragmatic reasons, investigations on the aerodynamic features of automotive wheels in isolation had received rather little attention in the first half of the 20th century. The first aerodynamic study particularly based on isolated wheel of a car was performed by Morelli [7]. He measured forces acting on wheel assembly with direct method consisting of raising a wheel above a fixed floor and applying rotation to it. For the subsequent two decades, scientific papers mainly focused on the improvement of capturing the effects of ground contact [8] and circumferential pressure measurement accuracy [9].

The wheel aft flow structures were neglected until the first wind tunnel measurements targeted on wheel wake flow by Bearman et al. [10], aimed to visualise pressure distribution in a wake plane located 2.5 wheel diameters rear of the wheel using a pressure probe system.

Aerodynamic observations of a rotating wheel had been undertaken exclusively in wind tunnels until the work of Axon et al. [11], which was the first published CFD study on rotating wheel in isolation. Utilising computational methods for wheel aerodynamics was a major step towards automatized optimisation applications. This paper was followed by many studies focusing upon comparing and fine tuning different mesh and turbulence model types ([12], [13], [14]).

Knowles et al. [15] and Mears and Dominy [16] combined experimental and numerical practices in order to improve correlation between CFD simulation and real-life wind tunnel testing by evaluating the effect of changes in CFD set-up, with the output being validated against experimentally obtained data sets.

The first comprehensive work on wheel wake flow visualisation using CFD was delivered by McManus and Zhang [17]. They concluded that the flow structures behind rotating wheels are highly spatial, turbulent and immensely complex. They described an arch shaped ring vortex in the upper region, provoked by the separated flow at the top of the wheel tread. Additionally, counter rotating vortices are formed in the near wake region due to the '*horseshoe*' shaped separated flow at the leading edge of the ground contact.

Realising the importance of wheel wake flow fine tuning, Formula 1 team Scuderia Ferrari introduced front static wheel shrouds in the season of 2007, followed by many other teams. They have reported increased efficiency of diffusor and better cooling of wheel bearing and brake system. According to the work of Sprot et al. [18], wheel shrouds can decrease drag by 8.9% on the wheel assembly alone.

The popularity of overall drag reduction with optimised wheel geometry also arises among fully electric passenger car manufacturers with the very same intentions as FCE. For Tesla Model S, overall drag was decreased by 11% even so wheel wake induced drag is the fragment of open-wheel applications [19].

Automated shape optimisation of ground vehicles

First of all, optimisation is not to be confused with the practice of design of exploration or try-out of randomly selected configurations. These are indeed related to optimisation, but instead of trying to find the 'best possible' design, they compromise with a 'better' design [20].

Traditional aerodynamic shape optimisation is an iterative process between an aerodynamicist and a CAD designer. The proposed geometry modification for the next iteration is based on the evaluation of the previous version's aerodynamic results. The process is repeated until the set objective is reached. Optimisation could be written as a mathematical problem, which creates connection between a function (*f*) and the investigated design space (*S*):

$$f: S \rightarrow \mathbb{R}$$

$$f(x_{opt}) \leq f(x) \quad , where \quad \forall x \in S \quad and \quad x_{opt} \in S \quad (1)$$

In case of the shape optimisation of a bodywork affecting a highly three-dimensional and complex flow - such as a wheel pod – the cycle time would grow to infinitely large. Not to mention that finding the global minimum of a multi-dimension function is stretching the limit of human driven manual evaluation, leading to total uncertainty and mistrust regarding the discovery of the global minimum.

The first published scientific paper which combined direct, gradient-based optimisation methods with Navier-Stokes governing equations for an aerofoil was developed by Jameson et al. [21]. These types of optimisation algorithms are deterministic and can handle problems with only one minimum point by finding the optimal search direction [22].

There was a need to incorporate other optimisation strategies to overcome optimisation problems with multiple minima. Metaheuristics are problem independent, since they are modifying the parameters of the candidate shape both deterministically and randomly. The optimisation is guided by the elitist principle, taking the parameter sets with the best results into consideration with more weighting than the ones with inferior results. Metaheuristics originate from the Genetic Algorithm of Holland [23]. Therefore, the use of metaheuristics is an appropriate choice for aerodynamic shape optimisation of ground vehicle applications, based upon their performance. It is worth mentioning that the most aerodynamic shape is not inevitably the most aesthetic shape as well; in motorsport, this factor is usually neglected.

The first published evidence of metaheuristic optimisation was an aerodynamic development of the rear end of the Ferrari 360 Modena, delivered by Lombardi et al. [24]. The study focused on aerodynamic stability of the car. In motorsport, Singh and Golsch [25] presented the shape optimisation of the nose, tail and roof of a Pontiac NASCAR competition car to improve race track performance. They could realise almost 3% of downforce improvement with negligible drag increment.

This method has gained increasing popularity in the development of conventional passenger cars as well, mainly to effectively reduce fuel consumption. Aerodynamic optimisation of a Ford pick-up truck was undertaken by Lietz [26]. He reported very good and fast directional optimisation of the rear cab layout. Although he stated that fine tuning of the shape should be made manually, considering aesthetics.

Similar optimisations were carried out by Sun et al. [27] to find the best possible contours of the front and rear cross sections on a SUV in early stage of design. Total drag coefficient could be reduced by 0.018 in absolute value.

A recent application by Xu et al. [28] presented a multi-objective optimisation of the external shape of a high-speed train, and they achieved more than 9% of overall drag reduction.

Published metaheuristic driven ground vehicle aerodynamic optimisations are still infrequent, especially among motorsport applications. Thus, this scientific study has relevance in the field of aerodynamic shape optimisation.

The aim of this scientific study is to optimise front wheel pod geometry in order to reduce overall aerodynamic drag by at least 10% and eliminate front wheel generated lift force.

The main objectives and the layout of this scientific work are the following:

- Development of a validated CFD simulation of the full-scale car with zero yaw condition.
- Establishment of a metaheuristic aerodynamic optimisation framework to automatically control and manipulate a highly flexible and robust wheel pod geometry within the previously validated CFD simulation.
- Evaluation of the aerodynamic optimisation results and parameter sensitivity. Further, undertake a critical comparison of the coherent flow structures between the standard and best wheel pod design of the FCE car.

Methodology

Simulation method

Star-CCM+ 10.04.011R8 CFD simulation software was used to visualise and evaluate coherent flow structures and to determine the aerodynamic loads. Simulations were executed on a workstation featuring 20 cores of 3.1GHz Intel Xeon processors and 64GB of RAM at Oxford Brookes University.

In some cases, rotating wheel related scientific works simplify the problem by neglecting the rest of the vehicle focusing upon the wheel assembly ([9], [16]). Wheel wake flow does not only affect the wheel assembly itself. It is crucial in this case to solve the flow domain with the whole car, since the overall drag force is the function of the interaction between the modified wheel wake flow and other parts of the chassis as outlined by Newbon et al. [29].

According to Sprot et al. [18] the shape of wheel rim spokes and brake disks affect the magnitude of inlet spillage, while suspension rods can provoke large separations. As a result, they have extensive influence on the flow behind the wheel. Therefore, these parts of the suspension front and rear are taken into consideration along with the underbody, sidepod and helmet. Albeit, the level of detail of the CAD model must compromise between computational time and fidelity to real-life conditions. Internal volumes, narrow gaps and minor protrusions are neglected (Figure 3). The model also incorporates a constant deformation of the tyres near the contact patch, calculated at a certain speed, load and tyre stiffness, in order to imitate real-life conditions better [15]. Both camber effect and material elasticity of the tyres are disregarded, due to their small scales.

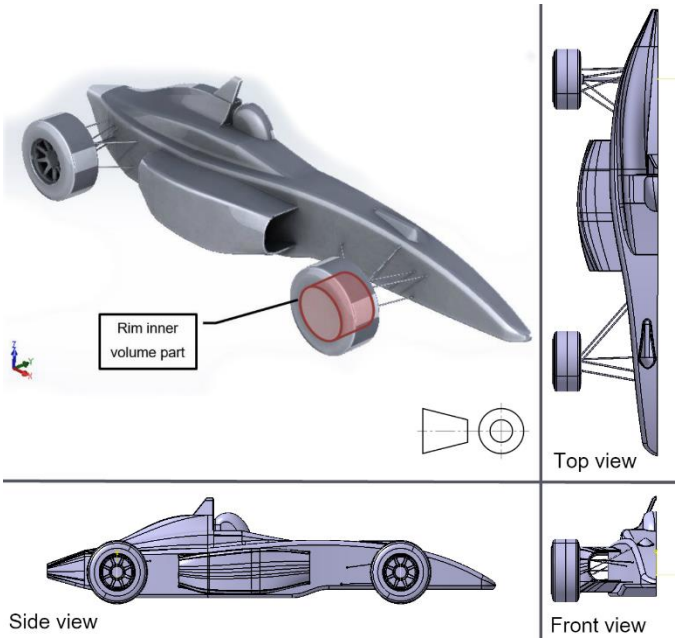

Figure 3. Simplified CAD model used for flow domain generation

Drag reduction of the FCE car has greater benefit at high speeds, since aerodynamic drag is proportional to the velocity squared. High speeds are predominantly typical at straight lines, thus yawed and steered conditions were disregarded. The flow domain was simplified by considering only one half of the virtual wind tunnel environment

at a 30ms^{-1} constant average straight-line speed extracted from Lap Time Simulations (Figure 4).

The extent of the virtual wind tunnel was adjusted to avoid 'pumping' effect caused by the apparent choke by the car geometry. Therefore, the total length was set 10 times the length of the FCE car. Hence, the inlet area was verified by the blockage ratio. In this case, a blockage ratio of 2.7% was found to provide good fidelity, corroborating the results of others ([30], [18]).

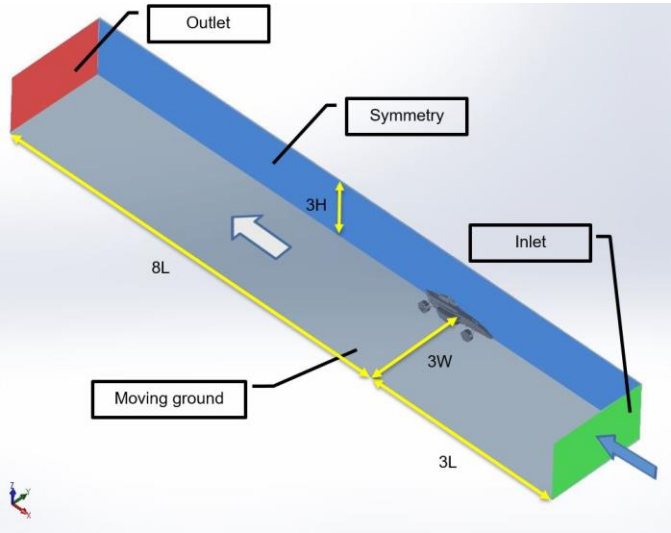

Figure 4. Setup of the virtual wind tunnel

Literature suggests that LES and VLES numerical solver methods provide better agreement with wind tunnel measurements, especially in the case of complex transient flow fields ([31], [32], [33]), but these methods converge to a result ten times slower on average when compared with a traditional RANS solver method.

Because of the good compromise between computational time and fidelity, the unsteady RANS method is mostly used for aerodynamic shape optimisation of ground vehicles as reported by Lietz [26] and Xu et al. [28]. Due to relatively limited computational resources, the CFD study of the candidate shape was based on the implicit unsteady RANS solver method with standard k-ε turbulence model.

Since wheel wake flows are highly turbulent and unsteady, it was necessary to incorporate time-dependency and geometry motions at specified volumes and surfaces. To apply corresponding tangential velocity at the front wheel rim, separate Local Reference Frame had to be introduced with a separate inner rim volume (Figure 5). Flux transport is enabled between the non-conformal interfaces. Furthermore, the duration of the simulated physical time must be long enough to capture full oscillation periods of the fluctuating wheel wake flow. At the same time, it must be minimised to lower cycle time. Investigations show that the specific dominant frequency of the oscillating flow is around 40 Hz, thus within five full rotations the drag force can be measured appropriately. As a result, the physical time of each simulation is nearly 0.28s.

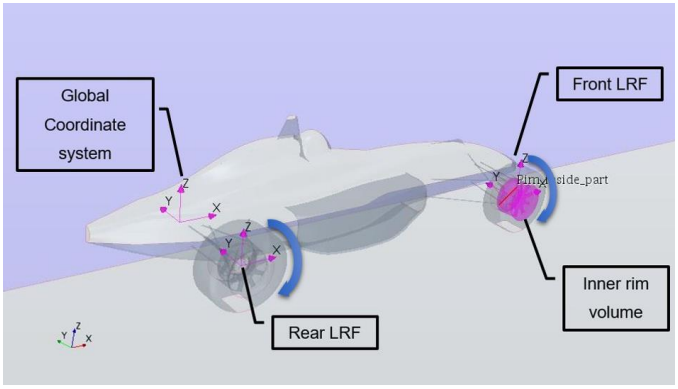

Figure 5. Location of global and local coordinate systems including assigned motions

The rather complex flow domain has enormous extent and features very detailed parts with high gradients and contractions, thus it was essential to develop five sub-regions with individual volumetric control to ensure the ideal cell size, growth rate and boundary layer set-ups (Figure 6).

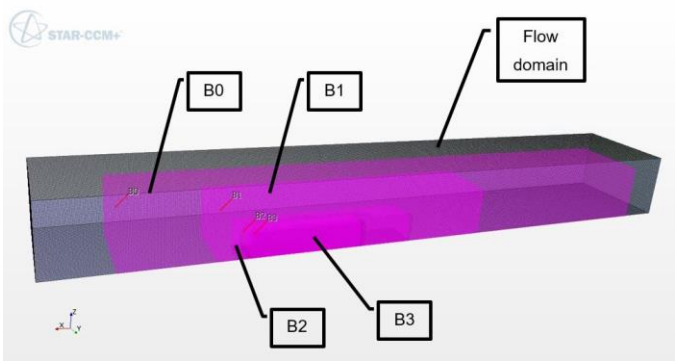

Figure 6. Assembly of sub-regions

For the present study, unstructured hexahedral meshing technique was used, coupled with structured prism layers. This type of meshing

provides the lowest cell count per unit volume ratio while it provides good numerical stability for transient flows [34]. Table 1 contains the mesh set-up parameters for each volume.

Table 1. CFD meshing set-up parameters for each sub-regions

Regions	Flow domain				Rim inner
Sub-regions	B0	B1	B2	B3	-
Base size [mm]	100				5
Remesher [% to Base]	60	40	30	5	-
Max. cell size [% to Base]	150				150
No. prismatic layers	5				5
Thickness of BL [mm]	5				5
Prismatic layer stretch	1.2				1.2
Template growth rate	Slow				Slow

In order to guarantee acceptable solution for the boundary layer, the best practice is to employ a modelling function for the velocity profile within the boundary layer region rather than resolving the boundary layer in full numerically. The wall Y+ values on the surfaces must be verified that they are within the log-law region (500>Y+> 30) and homogeneous [35].

The setup parameters were adjusted during the validation process of the unsteady RANS simulation. The objective was to stay within 10% of correlation between C_{dw} values and the extents of pressure contours on specified span-wise probe planes compared with relevant wind tunnel publication results [18], [5], [36].

Figure 7 displays the location of the post processing planes. The wake flow examination will rest on stagnation pressure coefficient, relative stream-wise velocity and Lambda-2 vortex criterion visualisations.

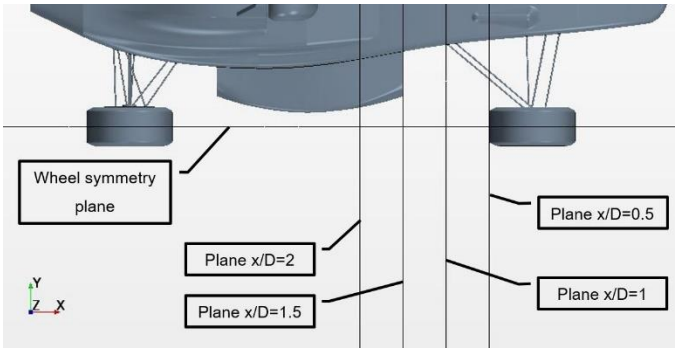

Figure 7. Location of post processing planes

Optimisation method

The previously introduced CFD model is completed with a parametric wheel pod geometry. Both of them form the candidate geometry which allows the optimisation algorithm to modify its set of parameters. During the design of the wheel pod geometry the following aspects need to be considered:

- Physical limitations
- Aerodynamic concerns
- Robustness
- Manufacturing
- Maintenance

The wheel pod geometry must avoid any collisions with the moving ground, rotating wheel or other parts of the FCE car in any conditions. Furthermore, the wheel pod must not increase the frontal area of the car, therefore needs to be within the frontal contour of the wheels. Also, the parametric wheel pod must be robust; meaning that CAD model generation collapse is forbidden in case of any possible candidate shape permutations. Finally, the part design should allow easy manufacturing and maintenance, without increasing moment of inertia of the car considerably. In order to sketch the preliminary wheel pod geometry, typical wake flow structures were examined around the isolated wheel (Figure 8).

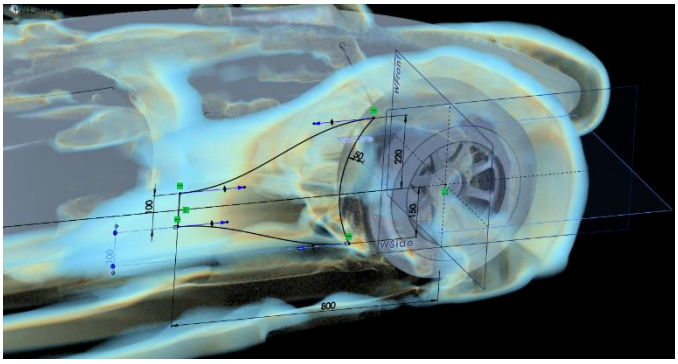

Figure 8. Three dimensional initial sketch of the wheel pod guided by lambda-2 vortex criterion

Figure 9 displays the seven driving parameters of the wheel pod. HU and HL control the position of the leading edges of the wheel pod. The trailing edge is driven by HB and HR is guiding the 'flatness' of the pod. The connection between these edges are realised by NURBSs. ALFA is responsible for the asymmetry of the wheel pod, while BETA defines the draft angle of the bodywork. The range of these parameters were selected with respect to the design aspects.

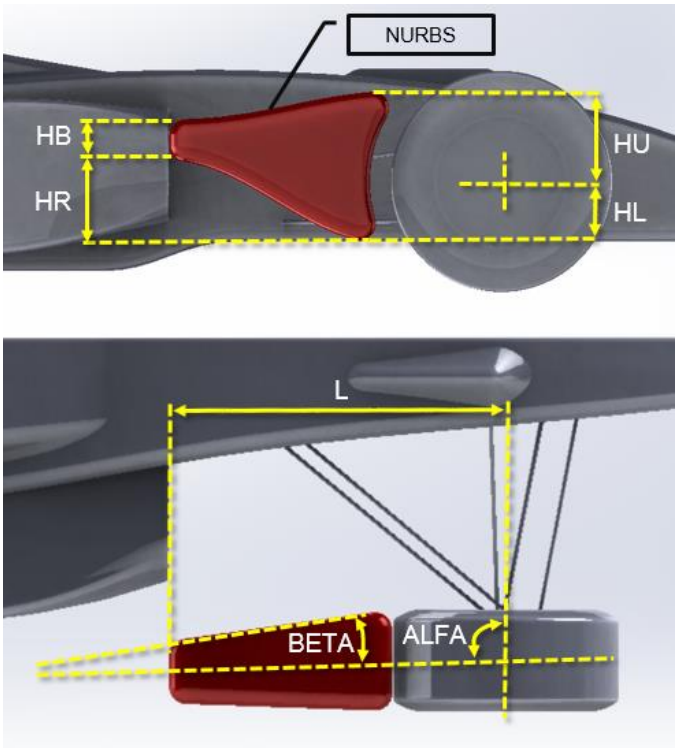

Figure 9. Locations of the wheel pod governing parameters

The aim of this study tolerates the use of single-objective optimisation. The search evaluation is based on the value of C_d with a target to minimise. The function of the surface where the global minimum is searched is 8-dimensional and to overcome unrealistic results, upper and lower constraints are set to C_d.

The aerodynamic optimisation is executed through a third-party software, called HEEDS MDO. This optimisation tool allows the user to select from different types of search algorithm and fine tune their parameters. For the optimisation of the wheel pod, SHERPA is selected. According to Chase et al. [38], SHERPA reaches the global minimum of a multi-dimensional surface twice as fast as the second-best ASA.

For the number of total iterations Lietz [26] suggested five times, Sun et al. eight times the number of driving parameters. In this study, 40 iterations are assigned for an optimisation batch.

Figure 10 shows the overview of the optimisation loop. Initially, CFD solutions are generated for a group of randomly selected candidate shapes. The hybrid search algorithm ranks the best designs and evaluates the relation between the results and the parameter values. This process is performed with the simultaneous work of multiple metaheuristic global algorithms and deterministic local search algorithms. Successful individuals are more likely to transmit their chromosome segments for the next generation. The best designs with different chromosome segments are forming crossover. Mutation of a randomly selected chromosome is needed to avoid misleading convergence towards a local minimum.

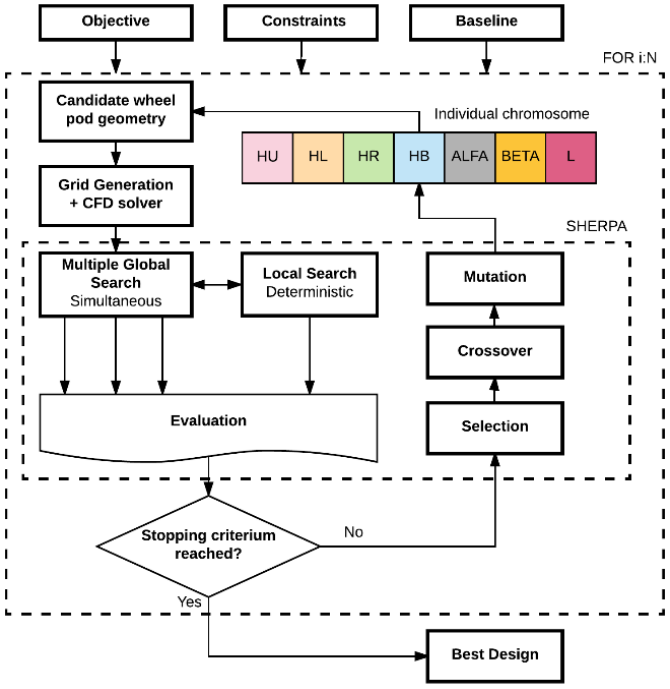

Figure 10. Structure of the optimisation process

In order to visually analyse and understand the correlation between design parameters and C_D response, Kriging surrogate surface model is applied. Kriging model is a widely-used optimisation process which combines regression and correlation model, entailing good surface approximation for the whole design space based on random output data.

Results and Discussion

Geometry evolution

The importance of geometry and CFD model robustness is essential for adequate optimisation results. In the case of the Set 1 optimisation batch, 22% of all simulations collapsed due to unsuccessful geometry and/or grid creation. Based on this experience, a refined CAD model tree and grid setup were integrated into the next optimisation batch process. The optimisation time was 200 computational hours for a complete data set.

Figure 11 shows the objective history of the two separate processes. It can be seen that in both cases, the convergence of the objective history is fairly similar. The first half of the graph demonstrates abrupt gain in reducing total drag. The second half of the graph indicates highly vigorous mutating and crossover attempts of the search algorithm. This endeavour, to find a supposed better was successful, leading to Design #33 proved to be the most desirable wheel pod geometry, since it has the lowest drag coefficient. Increasing variance in drag output indicates more aggressive mutations, but further drag reduction was unsuccessful. The obviously found minimum may be a global minimum for the 8-dimension function. Based on the visible convergence of the objective history, using the second order polynomial fitting technique, the predicted minimum of the function is at 45 iterations with a 0.6% additional Cd reduction.

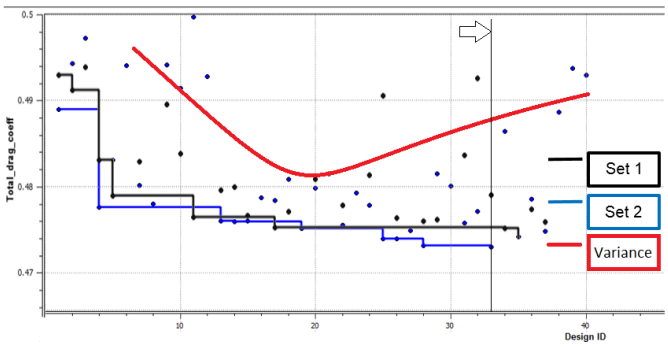

Figure 11. Objective history graph

Figure 12 displays how the shape of the wheel pod evolved during the optimisation process. Five generations can be distinguished, based on the typical layout of the cycles. Baseline employed long and bulky pod design. It was followed by short, cornered tailing design with high upper leading edge. The Cd improvement was the greatest in average (more than 2%) in this case. The second generation is the modified version of the first, featuring a pointed tail design and lower upper leading edge. The third generation changed the length and the draft angle of the pod. The fourth generation is where the best Design #33 is reached. The wheel pod became symmetric, slightly drafted and flat bottomed above the features of the third generation. The fifth generation shows extravagant shape changes. Some of the generated shapes replicate previous generation attempts and were confirmed to be less effective than the fourth generation.

Analysis of parameter variation

In order to understand the effect of each parameter change on the objective, a parameter analysis must be carried out with Pearson correlation coefficient. This widely used formula shows the lineal correlation between two common parameters ([39], [40]). The evaluation of the results helps to identify each parameter sensitivity; thus it supports further manual fine tuning of the wheel pod shape.

Table 2 shows the list of the Pearson correlation coefficients of the parameters towards drag. ALFA and L presented weak, while HL, BETA and HR medium correlation. HB and HU are the most influencing parameters. Noteworthy, there are some errors in parameter correlations due to the nature of linear approximation. For instance, L proved to have a negative correlation with drag, but the approximation calculated it as positive.

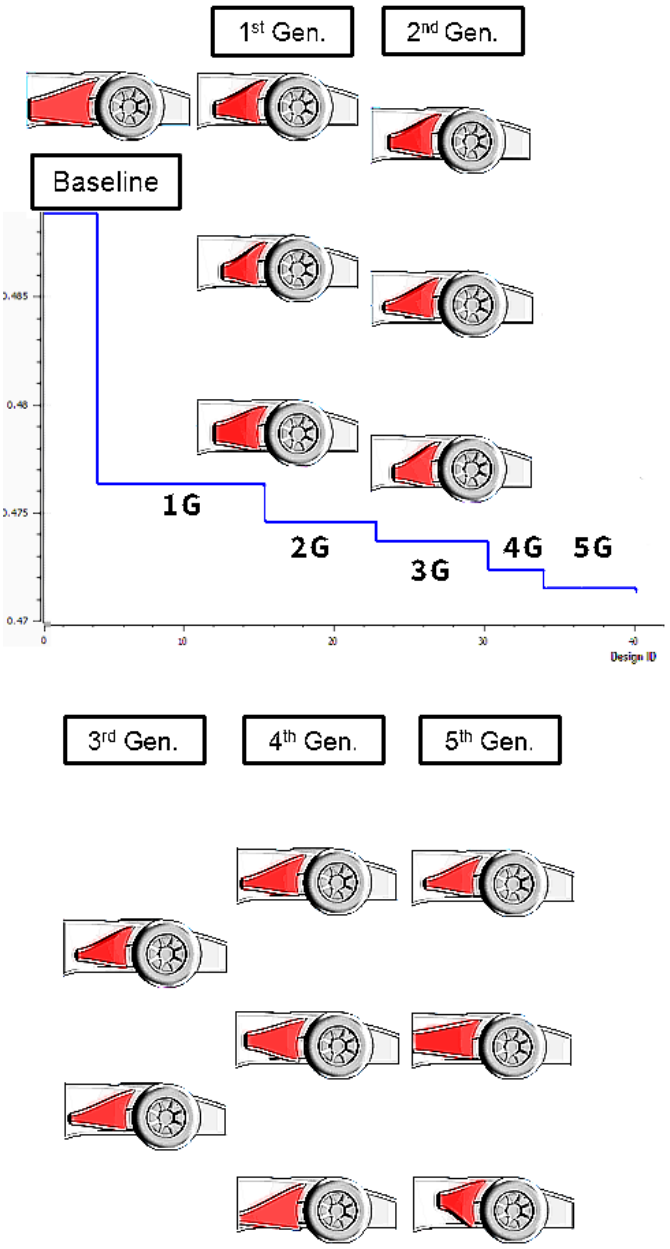

Figure 12. Wheel pod evolution during the optimisation process

Table 2. Pearson correlation coefficeint between each governing parameter and total drag coefficient

Parameter name	Pearson correlation coefficient on C_d
ALFA	0.01
L	0.12
BETA	-0.28
HR	0.40
HL	0.43
HB	0.55
HU	0.64

The end of the tailing is defined by HB and Figure 13 reflects the importance of this parameter on the velocity field behind the pod. The two designs, numbers 37 and 39, only differ in the value of HB, other parameters are all identical. The 'bulky' the wheel pod geometry results flow separations at the trailing edges. High relative stream-wise velocity fields behind the pod are indicating the formation of standing ring vortices, which is detrimental to drag reduction. In contrast, pointed tailing geometry demonstrates no evidence of a low-pressure zone behind the pod. This design is closer to highly aerodynamic 'teardrop' shapes.

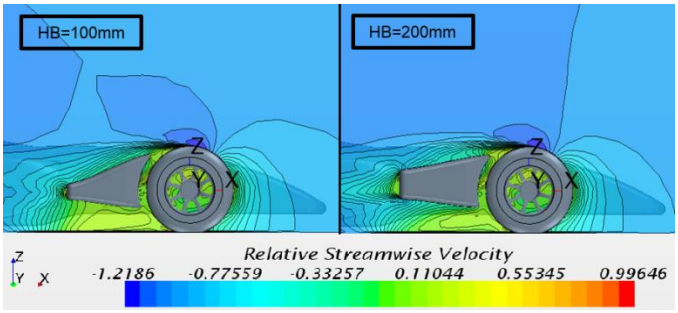

Figure 13. Relative streamwise velocity comparison of different tailing designs

HU is controlling the upper leading edge of the pod; therefore, it is in connection with the separated flow formed at the upper tyre surface. Again, two identical designs were selected (Design #1 and #34), with the only difference in HU. Figure 14 shows the how the reattachment location affects the induced drag force - described by Taniguchi et al. [41]. Tall design interferes with the hardly separated flow of the tyre, hence it leads to greater top surface angle, which increases the possibility of local separation and recirculation. Wider and taller stagnation pressure contours in case of tall upper leading edge design corroborates the hypothesis and indicates more induced drag.

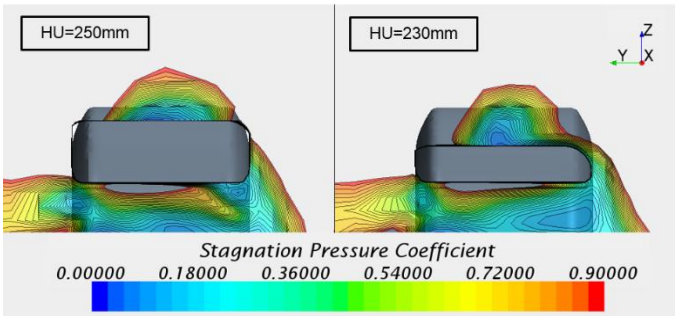

Figure 14. Stagnation pressure coefficient comparison of different upper leading edge designs

In the following, the effect of driving parameter pairs on the drag objective will be explained using the Kriging surrogate response surface modelling technique. One parameter is paired with another if their changes affect each other, producing an irregular response surface of drag. The correlation between HR and HU is the greatest, with positive 0.68. On Figure 15, the response surface has only one minimum at the lowest HU and HR values. It is visible that the effect of HU on C_d decreases by increasing the height of the tailing. Upwards pointing pod is highly unfavourable in contrast with flat bottomed pod design. As stated previously, a short upper leading edge entails better aerodynamic performance.

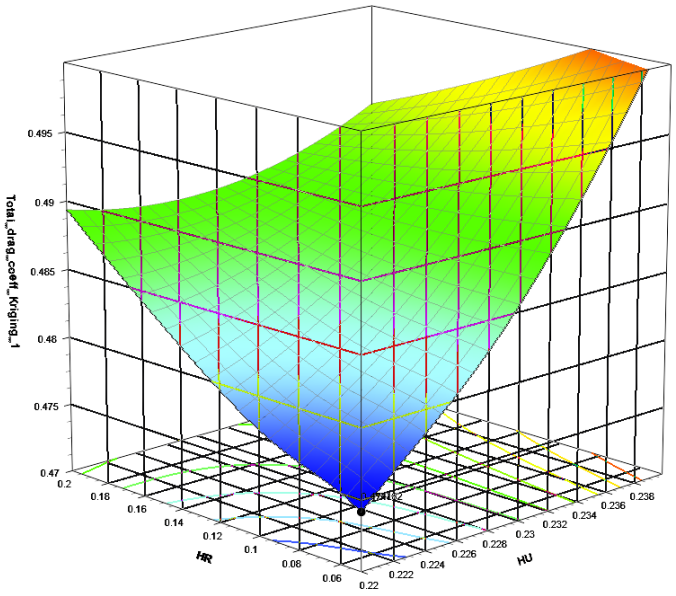

Figure 15. Kriging surrogate surface of HU, HR and total drag coefficient

The correlation between HL and BETA is -0.43, which means medium interaction. The response surface features two minima, both at median height of the lower leading edge (Figure 16). Wheel pod with lower than 0.2D HL conflicts with the recirculating vortex originated from the tyre shoulders near the ground contact. This corroborates the measurements of Mears [5].

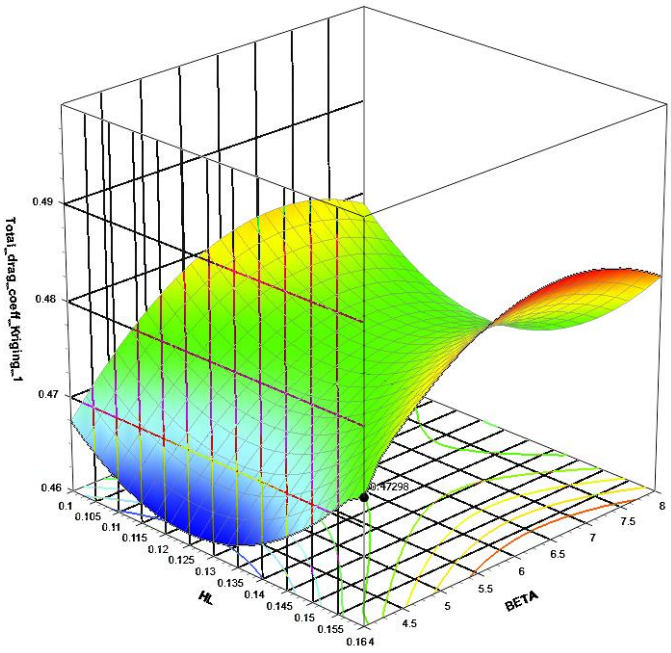

Figure 16. Kriging surrogate surface of BETA, HL and total drag coefficient

Figure 17 shows, that a wheel pod with higher lower leading edge is not able to prevent the reattaching flows under the wheel pod, due to the strong outwash effect from the chassis.

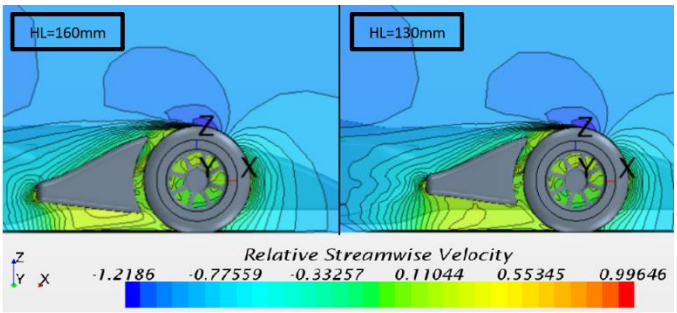

Figure 17. Relative streamwise velocity comparison of different lower leading edge designs

The explanation behind the apparent effect of BETA change is at issue. Based on the evaluations of CFD output, significant differences between various draft angles are not detectable. The imperfection of the Kriging surface fitting might be the answer, although it is not possible to answer at present.

Figure 18 displays the fitted Kriging response surface between ALFA and L. Both of them have low correlation to drag, but negative 0.39 between each other. It can be seen that longer wheel pod is preferable in most of the cases. Long bodywork diminishes the effect of the outward push from the leading edges of the sidepod.

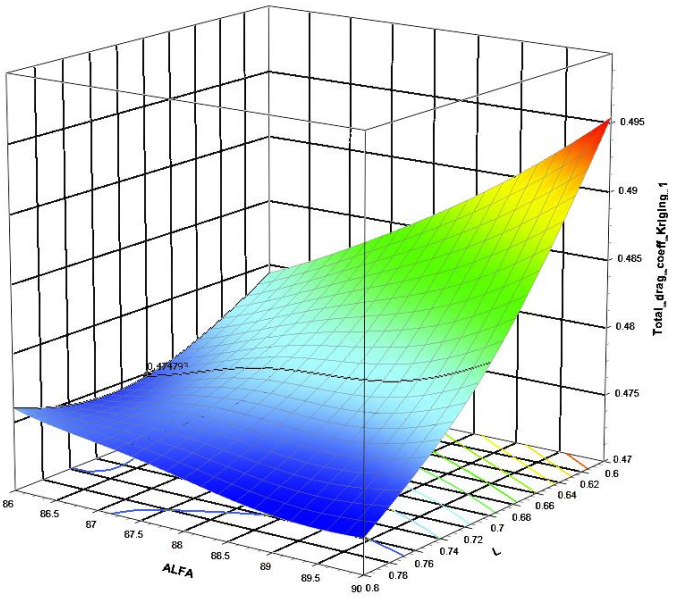

Figure 18. Kriging surrogate surface of L, ALFA and total drag coefficient

It is also visible, that symmetric design provides better drag reduction. Streamlines on Figure 19 demonstrate that heavily asymmetric, long versions have an inner recirculation, producing induced drag. Albeit, asymmetry is beneficial in case of short pod designs, but the overall C_d reduction is poor.

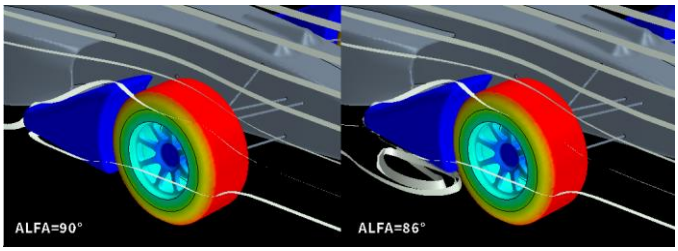

Figure 19. Streamline comparison of different longitudinally aligned designs

Comparison with original layout

Coherent flow structures around the car is investigated with Lambda-2 vortex criterion. Figure 20 displays the how the flows are modified around the FCE car with the utilization of the best wheel pod design. The baseline model features a highly yawed trailing vortex pair originated from the ground contact region. The outboard vortex passes by the FCE car 2.5D sideways. At the inboard side, the vortex conflict with the sidepod, then merge together with the upper wheel wake flow at 2.5D rearwards from the first axle. This highly turbulent, low pressure regime collides with the rotating surface of the rear wheel. This leads to a 0.D of amplitude oscillating flow behind the car.

When the design #33 wheel pod is applied, the trailing vortex pair is not visible anymore. Instead, a single anti-clockwise vortex is created beneath the pod. Upper wake flow can reattach onto the upper surface of the bodywork, thus minimising wake flow generation locally. The formed wake flow is smaller in extent and less turbulent (Figure A1). The rear wheel is approached by this less intense and straightened flow. The wake formation in length and expansion behind the rear wheel is halved. This corroborates the observation of Newbon et al. [29], that overall drag can be reduced by straightened flow towards the rear wheels.

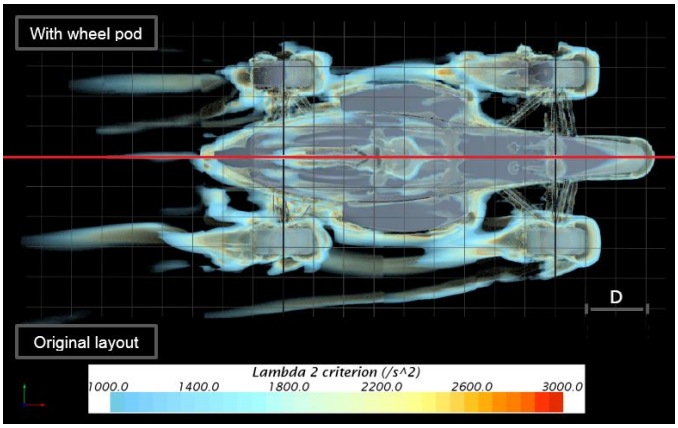

Figure 20. Lambda-2 vortex criterion comparison between the baseline and the optimised design

Table 3 contains the relative differences between the original FCE car and the FCE car with the best wheel pod design. The aerodynamic optimisation is successful, since the assigned 10% overall drag reduction aim is reached and at the same time the downforce is increased due to diminished lift forces of the front wheels. The 11.1% total drag reduction is mainly realised at the front wheels. Altogether, the aerodynamic efficiency is increased by 17.1%.

Table 3. Results summary of the aerodynamic optimisation

Aspect name	Relative difference to Baseline (Design #33)
Overall drag coefficient	-11.1%
Front wheels drag coefficient	-22.5%
Drag distribution of front wheels	-13.0%
Overall downforce	+4.2%
Lift / Drag ratio	+17.1%

Figure 21 shows the FCE competition car utilised with the best wheel pod geometry. The development of the support sting and the manufacturing of the wheel pod assembly are identified as possible future works.

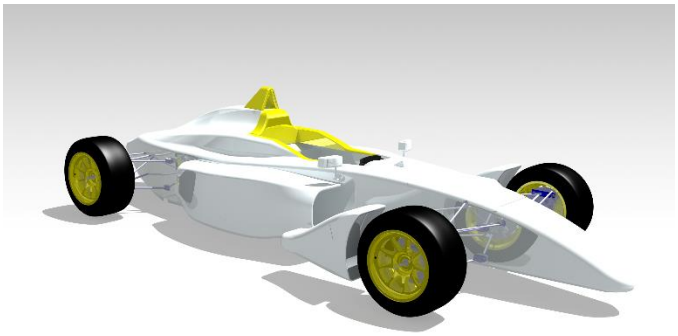

Figure 21. Rendered image of the FCE competition car with the optimised wheel pod

Summary

This scientific work focused on the development of a front wheel pod to reduce overall drag force without adversely affecting downforce generation. The exploration of the optimal wheel pod is executed by a single objective aerodynamic optimisation framework, coupled with validated CFD simulations. Overall drag of the FCE car could be reduced by 11.1% and at the same time downforce could be increased by 4.2%. The initially defined aim and objectives has been fully accomplished. The key finding of this scientific study are the followings:

- The frequency of oscillating wheel wake flow limits the reduction of simulation physical time.
- SHERPA search algorithm delivered acceptable objective history convergence within 40 iterations. Global minimum is certainly found for an 8-dimension function.
- Lengthy bodywork placed behind the front wheel can reduce drag more effectively.
- Symmetric wheel pod designs deliver more drag reduction, than asymmetric versions.
- Pointy tailed bodyworks can reduce the extent and the kinetic energy of trailing vortices.
- The detrimental effect of flow towards the rear wheels on drag is corroborated.
- Wheel pod can reduce lift forces of the front wheels, therefore increasing overall aerodynamic efficiency.

The optimised wheel pod bodywork allows competitive race track performance for the FCE race car against other internal combustion entry level formula racing cars.

References

[1] J. E. Maroti, Perception towards electric racing. MSc Thesis, Oxford Brookes University, 2017.

[2] FIA Formula E, 2017. Teams and Drivers. [ONLINE] Available at: http://www.fiaformulae.com/en/championship/teams-and-drivers/. [Accessed 11 June 2017]..

[3] A. Sprot, D. Sims-Williams és R. Dominy, "The Aerodynamic Characteristics of a Fully Deformable Formula One Wind Tunnel Tyre," SAE Int. J. Passenger Cars - Mech. Syst. 5(2): 2012..

[4] R. G. Dominy, Aerodynamics of Grand Prix Cars. Proc. Instn Mech. Engrs. Part D, 206D, 1992..

[5] A. P. Mears, The Aerodynamic Characteristics of an Exposed Racing Car Wheel. PhD Thesis, University of Durham, 2004..

[6] Biermann és Herrnstein, The Drag of Airplane Wheels, Wheel Fairings, and Landing Gears II: Nonretractable and Partly Retractable Landing Gears, National Advisory Committee for Aeronautics. Langley Aeronautical Lab.; Langley Field, VA, United States, 1936.

[7] A. Morelli, Aerodynamic Effects on an Automobile Wheel. Technical Report Trans. 47/69, MIRA, 1969..

[8] W. Stapleford és G. Carr, Aerodynamic Characteristics of Exposed Rotating Wheels. Technical Report 1970/2, MIRA, 1970..

[9] J. Fackrell és J. Harvey, The Flow Field and Pressure Distribution of an Isolated Road Wheel, Advances in Road Vehicle Aerodynamics. BHRA Fluid Engineering Conference - Paper 10, 1973..

[10] P. Bearman, D. De Beer, E. Hamidy és J. Harvey, The effects of a moving floor on wind-tunnel simulation of road vehicles. SAE880245, 1988..

[11] L. Axon, K. Garry és J. Howell, An Evaluation of CFD for Modelling the Flow Around Stationary and Rotating Isolated Wheels. SAE 980032. 1998, 65-75..

[12] A. Skea, P. Bullen és J. Qiao, The use of CFD to Predict Air Flow Around a Rotating Wheel. 2nd MIRA International Conference on Vehicle Aerodynamics. 1998..

[13] W. Kellar, S. Pearse és A. Savill, Formula 1 Car Wheel Aerodynamics. Sports Engineering. 1999, 2, 203-212..

[14] M. Hinson, Measurement of the Lift Produced by an Isolated, Rotating Formula One Wheel Using a New Pressure Measurement System. MSc Thesis, Cranfield University: College of Aeronautics. 1999..

[15] R. Knowles, A. Saddington és K. Knowles, Simulation and experiments on an isolated racecar wheel rotating in ground contact. 4th MIRA International Conference on Vehicle Aerodynamics, 2002..

[16] A. Mears és R. Dominy, "Racing Car Wheel Aerodynamics – Comparisons between Experimental and CFD Derived Flow-Field Data," SAE Technical Paper 2004-01-3555, 2004, doi:10.4271/2004-01-3555..

[17] J. McManus és X. Zhang, A Computational Study of the Flow Around an Isolated Wheel in Contact With the Ground. ASME J. Fluids Eng., 128, pp. 520-530.

[18] A. Sprot, J. Minto, D. Sims-Williams és R. Dominy, "Aerodynamic Investigation on the Effect of Varying Through-Hub Flow on a Formula One Front Wheel Assembly," SAE Int. J. Passeng. Cars – Mech. Syst. 4(1):929-944, 2011, doi:10.4271/2011-01-1431..

[19] A. D'Hooge, R. Palin, S. Johnson és B. e. a. Duncan, "The Aerodynamic Development of the Tesla Model S - Part 2: Wheel Design Optimization," SAE Technical Paper 2012-01-0178, 2012, https://doi.org/10.4271/2012-01-0178..

[20] D. Thévenin és G. Janiga, “Optimization and Computational Fluid Dynamics”, Springer-Verlag Berlin Heidelberg, 2008, ISBN 978-3-540-72152-9..

[21] A. Jameson, L. Martinelli és N. Pierce, Optimum aerodynamic design using the Navier-Stokes equations. Theoretical and Computational Fluid Dynamics. 10(1–4), 213–237. 1998..

[22] R. Carrese, Identifying preferred solutions for multi-objective aerodynamic design optimization, Doctor of Philosophy (PhD), Aerospace Mechanical and Manufacturing Engineering, RMIT University. 2012..

[23] J. H. Holland, “Adaptation in natural and artificial systems”, Univ. Of Michigan Press, Ann Arbor, MI, 1975..

[24] G. Lombardi, H. Vicere, H. Paap és G. Manacorda, “Optimized Aerodynamic Design for High Performance Cars”, AIAA-98-4789, MAO Conference, St. Louis, 1998..

[25] R. Singh és K. Golsch, "A Downforce Optimization Study for a Racing Car Shape," SAE Technical Paper 2005-01-0545, , doi:10.4271/2005-01-0545. 2005..

[26] R. Lietz, "Vehicle Aerodynamic Shape Optimization," SAE Technical Paper 2011-01-0169, 2011, doi:10.4271/2011-01-0169..

[27] S. Sun, Y. Chang, Q. Fu, J. Zhao és et al., "Aerodynamic Shape Optimization of an SUV in early Development Stage using a

Response Surface Method," SAE Int. J. Passeng. Cars - Mech. Syst. 7(4), 2014. doi:10.4271/2014-01-2445..

[28] G. Xu, X. Liang, S. Yao, D. Chen és Z. Li, Multi-Objective Aerodynamic Optimization of the Streamlined Shape of High-Speed Trains Based on the Kriging Model. PLoS ONE 12(1): e0170803. 2017..

[29] J. Newbon, D. Sims-Williams és R. Dominy, "Aerodynamic Analysis of Grand Prix Cars Operating in Wake Flows," SAE Int. J. Passeng. Cars - Mech. Syst. 10(1):2017, doi:10.4271/2017-01-1546..

[30] A. Singh, S. Kumar és K. Nikam, High Performance CFD Computations for Ground Vehicle Aerodynamics. SAE Technical Paper Series, 2011..

[31] B. Schnepf, “Untersuchung von Einflussfaktoren auf die Umströmung eines Pkw-Rades in Simulation und Experiment”, PhD Thesis, Technical University of Munich, December 2015..

[32] C. Lew, N. Gopalaswamy, R. Shock és B. e. a. Duncan, "Aerodynamic Simulation of a Standalone Rotating Treaded Tire," SAE Technical Paper 2017-01-1551, 2017, doi:10.4271/2017-01-1551..

[33] J. Axerio, G. Iaccariono, E. Issakhanian, K. Lo és et al., "Computational and Experimental Investigation of the Flow Structure and Vortex Dynamics in the Wake of a Formula 1 Tire," SAE Technical Paper 2009-01-0775, 2009, doi:10.4271/2009-01-0775..

[34] CD Adapco, User Guide STAR-CCM+ Version 8.06. 2013..

[35] J. Middendorf, Modeling of wind tunnel flow over a rotating cylinder. Project Report, 2003..

[36] A. Wäschle, S. Cyr, T. Kuthada és J. Wiedemann, Flow Around an Isolated Wheel – Experimental and Numerical Comparison of Two CFD Codes. SAE2004-01-0445, 2004..

[37] M. Diosy, “Aerodynamic Optimisation of Front Wheel Pod for Formula Club E Competition Car using Metaheuristic Approach”, MSc Thesis, Oxford Brookes University, 2017.

[38] N. Chase, M. Rademacher, E. Goodman, R. Averill és R. Sidhu, “A Benchmark Study of Optimisation Search Algorithms”, Red Cedar Technology, 2010..

[39] K. Pearson, “Notes on Regression and Inheritance in the case of two parents”, Proceedings of the Royal Society of London, June 1895..

[40] F. Mariani, F. Risi, N. Bartolini, F. Castellani és et al., "Spoilers Optimization to Reduce the Induced Stresses on a Racing Helmet," SAE Technical Paper 2016-01-1612, 2016, doi:10.4271/2016-01-1612..

[41] K. Taniguchi, A. Shibata, M. Murakami és M. Oshima, "A Study of Drag Reduction Devices for Production Pick-up Trucks," SAE Technical Paper 2017-01-1531, 2017, doi:10.4271/2017-01-1531..

Contact Information

Definitions/Abbreviations

ASA	Adaptive Simulated Annealing
CAD	Computer Aided Design
C_d	Total drag coefficient
C_{dw}	Wheel drag drag
D	Wheel diameter [m]
GA	Genetic Algorithm
H	Overall height of the car [mm]
L	Overall length of the car [mm]
LES	Large Eddy Simulation
LRF	Local Reference Frame
LTS	Lap Time Simulation
NLPQL	Non-Linear Sequential Quadratic Programming
NURBS	Non-Uniform Rational Basic Splines
RANS	Raynolds Averaged Navier-Stokes
SHERPA	Simultaneous Hybrid Exploration
VLES	Very-Large Eddy Simulation
W	Overall width of the car [mm]

Appendix

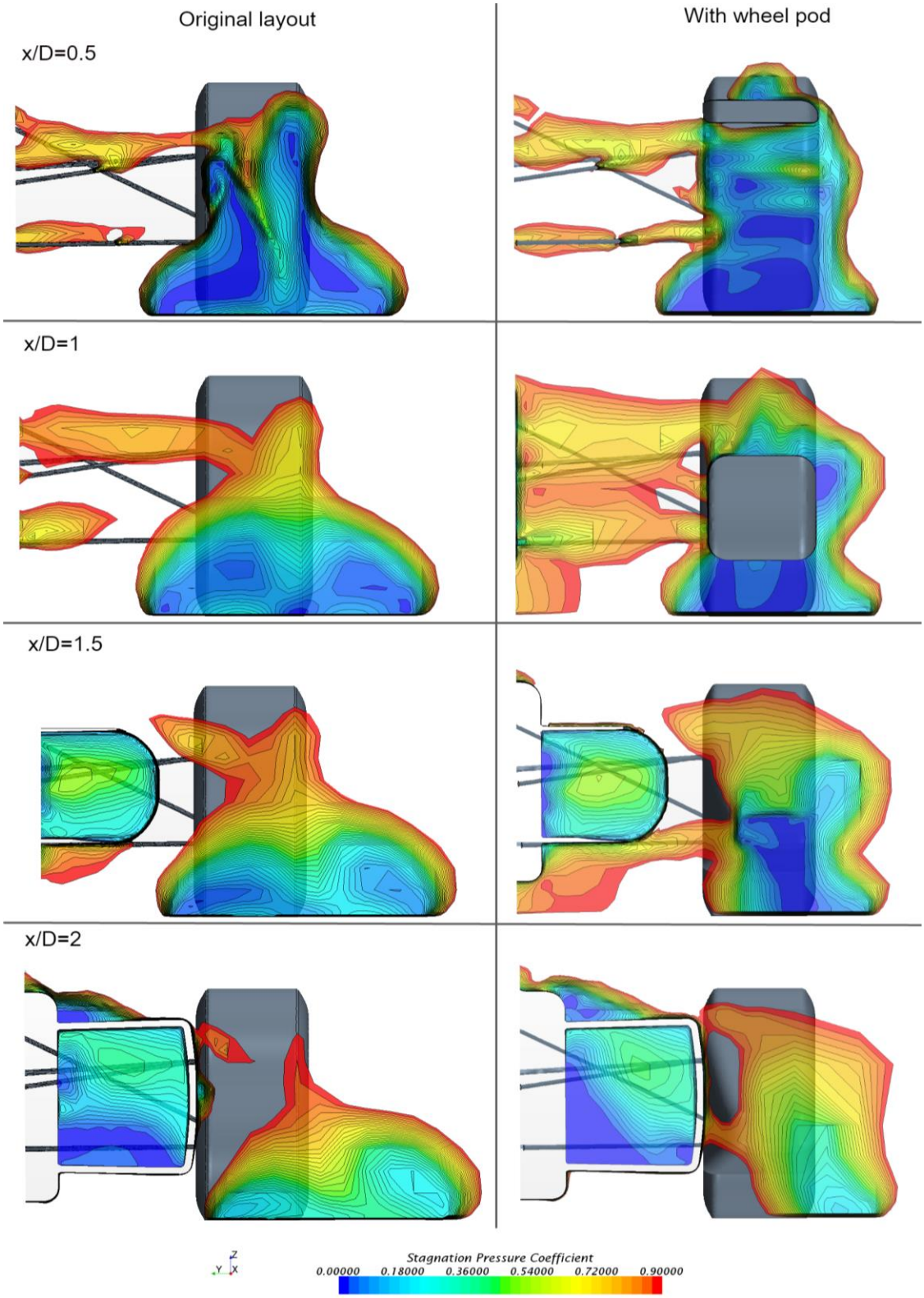

Figure A1. Stagnation pressure coefficient contours comparison between the baseline and the optimised design